

Spectral engineering of lithographically-scribed channel waveguide gratings

C. Greiner*, D. Iazikov and T. W. Mossberg
LightSmyth Technologies, Inc., 860 W. Park St., Ste 250, Eugene, OR 97041

ABSTRACT

We propose and demonstrate a powerful new approach to spectral bandpass engineering (apodization) of one-dimensional channel-waveguide Bragg reflectors. Bandpass engineering is accomplished via precise photolithographic control over the transverse width and longitudinal placement of individual grating lines which, respectively, provide unique line-by-line diffractive amplitude and phase control. Several channel waveguide gratings exhibiting complex filtering functions based on the present apodization method have been fabricated and modeled. They include an essentially polarization -insensitive 4-nm wide flat-top filter with steep roll-off and a multi-passband spectral decoder, useful, e.g., for optical spectral code-division multiplexing or spectral signature recognition. When a second-order apodization effect, comprising effective waveguide refractive index variation with grating-line transverse width, is included in the simulation, extraordinary agreement between predicted and observed spectral passband profiles is obtained.

Keywords: Integrated Optics, Photonic Crystals, Fiber Optics, Waveguide Grating, Distributed Bragg Reflector, Planar Lightwave Circuit, Photonic Bandgap Materials, Channel Waveguide, Apodization, Lithography, Silica-on-Silicon, Holography.

1. INTRODUCTION

Lithographic fabrication of one-dimensional, channel-waveguide Bragg reflectors constitutes a highly promising pathway to the low-cost volume production of robust and integrated optical filters. An inherent strength of Bragg reflectors is that, in principle, they can be designed to implement a broad range of spectral filtering and processing functions. In the limit of weak reflectivity, the Bragg grating's reflection spectrum is simply related to the spatial Fourier transform of the effective reflection coefficient expressed as a function of position into the grating. Obtaining control over the reflective amplitude and phase of grating-constituent diffractive elements makes possible the engineering of arbitrary phase-coherent spectral transfer functions. While the relationship between grating reflection spectrum and diffractive element amplitude and phase is more complex for strongly reflective gratings, the ability to implement broad ranges of filtering functions remains. Key to the engineering of specific filtering and processing functions is the ability to precisely control reflective amplitude and phase as a function of depth into the grating – even down to the level of individual grating lines.

The tailoring of spectral filtering functions has been previously demonstrated for fiber Bragg gratings [1-7] and channel-waveguides [8-10] by a variety of techniques. To date, none of the demonstrated methods provide for very high resolution (approaching line-by-line) control of diffractive element amplitude and phase. Recently, we proposed [11] and demonstrated [12] that photolithographic writing of *slab*-waveguide-based 2D Bragg structures provides a powerful pathway to controlling the reflective amplitude and phase of grating contours on a truly line-by-line basis. In the apodization method demonstrated, reflective amplitude control was based on partial (interrupted) writing of diffractive

* e-mail: cgreiner@lightsmyth.com; phone: (541)-431-0026; fax: (541)-284-5607

contours. An inherent advantage of this approach is its full compliance with a straightforward-to-implement fabrication process that employs one uniform etch depth. In the present paper, we demonstrate a different apodization approach useful for 1D lithographically-scribed Bragg gratings contained in channel waveguides. The method is based on controlling the reflective amplitude of individual grating lines by adjusting the fraction of the channel waveguide width that they span. Phase control of reflected light is achieved via spatial displacement of diffractive elements (grating lines) along the waveguide axis. The present channel-waveguide grating apodization method is, to our knowledge, unprecedented in its ability to manipulate reflective amplitude and phase of individual grating lines and is fully compatible with simple photolithographic fabrication methods.

2. RESULTS AND DISCUSSION

Figure 1a is a schematic cross section of the silica-on-silicon channel-waveguide Bragg grating. Diffractive elements (grating lines) are shown scribed in the interface between the waveguide core and the upper cladding layer. The grating lines are oriented perpendicular to the figure plane. The silica channel waveguide containing the Bragg grating consists of a rectangular, $6.4 \mu\text{m}$ (width w) \times $2 \mu\text{m}$ (height h) central core. The core's index contrast relative to the surrounding cladding layers (with $\geq 15 \mu\text{m}$ thickness) is $+0.8\%$. The grating diffractive elements are trenches, with depth $d \approx 400 \text{ nm}$, created by etching into the core and subsequently filling with cladding material. The grating operates in first diffraction order with a period, Λ , of about 500 nm , i.e. half the in-medium wavelength of resonant light.

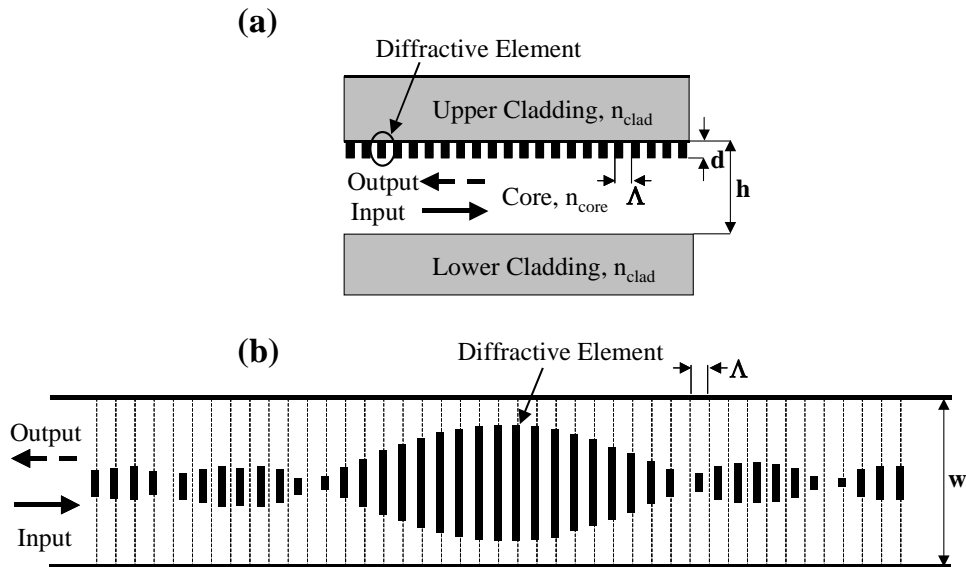


Figure 1. (a), Schematic cross-sectional view (cut plane perpendicular to grating lines) of the channel-waveguide Bragg reflector. (b) Schematic top view (looking down on grating trenches). d , grating depth, $h(w)$, waveguide core height (width), Λ , grating period. The apodization function shown is exemplary and different from those implemented in fabricated devices.

Figure 1b depicts a schematic view of a Bragg grating filter, apodized according to our method, showing diffractive elements as viewed looking down through the upper cladding. The optical signal enters the filter from the left side. The resonant input beam interacts with the diffractive elements of the Bragg grating (thick solid lines) and is coherently backscattered anti-parallel to the input. In Figure 1b, the net reflected field, $E_r^k(\vec{r})$, from an individual diffractive element (line) k is proportional to the integral of the product between input field $E_{in}(\vec{r})$ and the line reflection coefficient $r_k(\vec{r})$ evaluated along the transverse width of the grating line, i. e.

$$E_r^k \propto \int_{\text{line } k} \vec{E}_{in}(\vec{r}) r_k(\vec{r}). \quad (1)$$

Amplitude apodization of grating-constituent elements may be achieved through control of the grating line reflection coefficient $r_k(\vec{r})$ by, for example, controlling the trench depth d or by controlling the line's transverse extent or both. Since the lithographic fabrication process strongly favors a uniform etch depth, amplitude apodization via control of grating line width as shown in Figure 1b is highly advantageous.

In the work reported on here, a desired amplitude and phase apodization profile was realized by controlling transverse grating line widths and longitudinal line placements, respectively. The apodization amplitudes were approximated by a range of 42 different discrete values – each corresponding to a particular grating-line transverse width. The transverse widths employed spanned the range of 0 to 4.1 μm with discrete values separated by 100 nm increments. The maximal transverse width employed was chosen to be about 2/3 of the waveguide width to safeguard against potential fabrication-induced misalignment between Bragg grating and channel waveguide. When the transverse dependence of the input field mode distribution is taken into account, the relationship between reflected field amplitude and transverse grating line width becomes nonlinear. In determining the precise line width to amplitude relationship, the modal field is assumed to have a Gaussian transverse distribution (1/e-half width of 3.35 μm). Figure 1b shows how phase control of an individual reflected field is achieved by displacing the corresponding diffractive elements by an appropriate spatial offset from the nominal $\lambda/2$ grating-period position (indicated as dashed thin lines). In this manner, arbitrary reflected field phase shifts can be achieved, with a $\pm\pi$ phase shift corresponding to a $\pm\lambda/2$ displacement to the left (+) or right.

To experimentally verify the reflectivity versus transverse linewidth relationship predicted by Eq. (1), we fabricated seven 5-mm-long channel waveguide gratings each having lines of a different constant transverse length. Transverse grating widths of 4.1, 2.7, 1.8, 1.2, 0.8, 0.6 and 0.4 μm were implemented. Relative reflectivities, $(E_r^k)^2$, of approximately 0, -3, -6, -10, -13, -16 and -20 dB, with respect to the transverse grating of 4.1 μm , were expected.

Figure 2a and 2b, solid squares (empty circles) show the measured (modeled) insertion loss and 3-dB bandwidths, respectively, of the seven fabricated test structures for TE input polarization. A fiber-to-die coupling loss of 0.6 dB is subtracted from the test results shown in Figure 2a. Model results shown are based on coupled-mode theory. In obtaining the model results, we adjusted the diffractive element coupling strength of the 5-mm-long model grating until the reflective bandwidth of the strongest fabricated test structure (with 4.1 μm design linewidth) matched the measured width of the corresponding grating. Measured and predicted values of insertion loss were then found to agree. For the modeling of insertion loss and bandwidth of all other gratings, grating lines of reduced diffractive amplitude, calculated relatively using Eq. (1), were employed. Optimum agreement between model and test results was obtained when the transverse grating width was modeled to be 80 nm wider than the design values. This is reasonable considering that the lithographic tools cannot write grating lines with square ends. Lithographic resolution results in a rounding and hence lengthening of the grating lines. Results shown in Figure 2 utilize the design transverse grating width plus a constant 80 nm increment. As is evident in Figure 2, the agreement between test results and fitted model is quite excellent, which clearly validates Eq. (1) and confirms its usefulness for the design of more complex grating structures. For the two smallest transverse grating widths, measured reflective bandwidth values deviate from model values. Optical evaluation of these gratings revealed that certain of their grating lines were missing – suggesting that the small line sizes used in those gratings were pushing fabrication limits. Physical flaws in those gratings are likely the cause of the observed excess spectral width.

In Figure 3a, we demonstrate application of the present apodization approach to the design and fabrication of a channel-waveguide Bragg filter with a 4-nm-wide (measured at -3dB) flat-top spectral passband. The grating has a length of about 1.1 cm, and, if fabricated with a constant pitch, would exhibit an unsaturated spectral linewidth of about 0.09 nm. In order to achieve the substantially larger passband demonstrated here, the grating period was chirped. An additional amplitude and phase apodization was employed to minimize passband ripple. The designed grating structure was laser-written to a reticle, whose patterns were transferred via DUV photolithography to the channel waveguide.

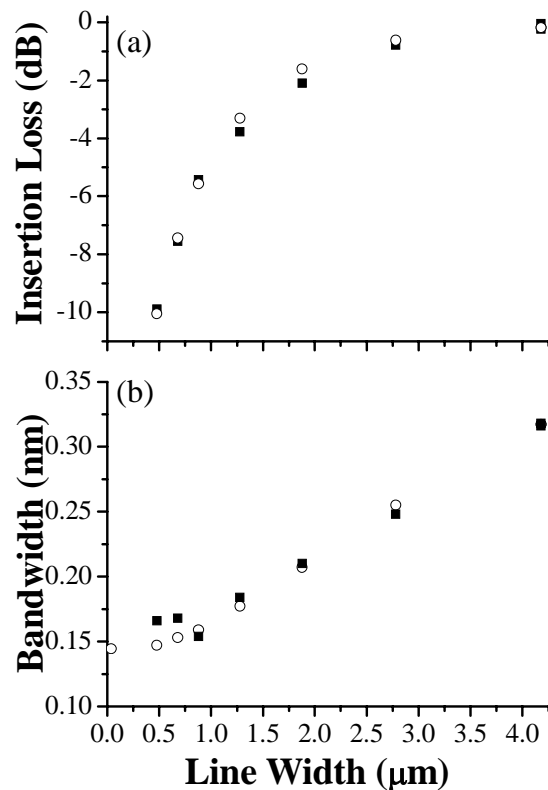


Figure 2. Insertion loss (2a) and 3-dB bandwidth (2b) versus linewidth. Solid squares, measurement; empty circles, model.

Figure 3a depicts the passband profile calculated from the design set of apodized grating lines using an extensive Fresnel-Huygens diffraction calculation. In this calculation, the effective refractive index of the channel waveguide is taken to be independent of the apodization. Figure 3b gives the measured spectral transfer function of the fabricated device for TE-polarized input light. The achieved passband profile closely reproduces the designed passband. The measured absolute insertion loss was ~ -8 dB which includes about 1dB for fiber-to-waveguide coupling. The slight passband ripple at the filter's short-wavelength side and the slower (compared to design) long-wavelength fall-off arise from a second-order apodization effect comprising an effective refractive index variation concomitant to amplitude apodization. Measurements performed on various test grating structures, each having grating lines of fixed transverse width, show a small and approximately linear variation of effective waveguide refractive index with grating amplitude (i.e. transverse grating line width). The fractional effective index difference between a waveguide without a grating and one with a structure of maximal transverse linewidth was found to be -2×10^{-4} . Figure 3c shows a passband profile calculated by Fresnel-Huygens diffraction theory and including the measured apodization-induced effective refractive index change. The simulation now clearly reproduces all features of the fabricated device.

To further demonstrate the advanced spectral filtering capability made possible by the present apodization approach, a coder/decoder for optical spectral code division multiplexing (OCDMA) was fabricated. The 19-mm-long grating is capable of generating or identifying a 15-color-chip spectral code with 8-bits high (7-bits low) that spans a total bandwidth of 15 nm. The color chips have a 1-nm spectral width. In order to span such a large spectral region, the grating period Λ is strongly chirped while the amplitude of diffractive elements is modulated during the chirp to encode distinct spectral chips. Additionally, tailored phase modulation is introduced to reduce spectral ripples that would otherwise affect the spectrum of the amplitude-modulated chirp employed. Figure 3d is a Fresnel-Huygens-diffraction-based calculation of the expected spectral code calculated without the effect of amplitude-apodization-

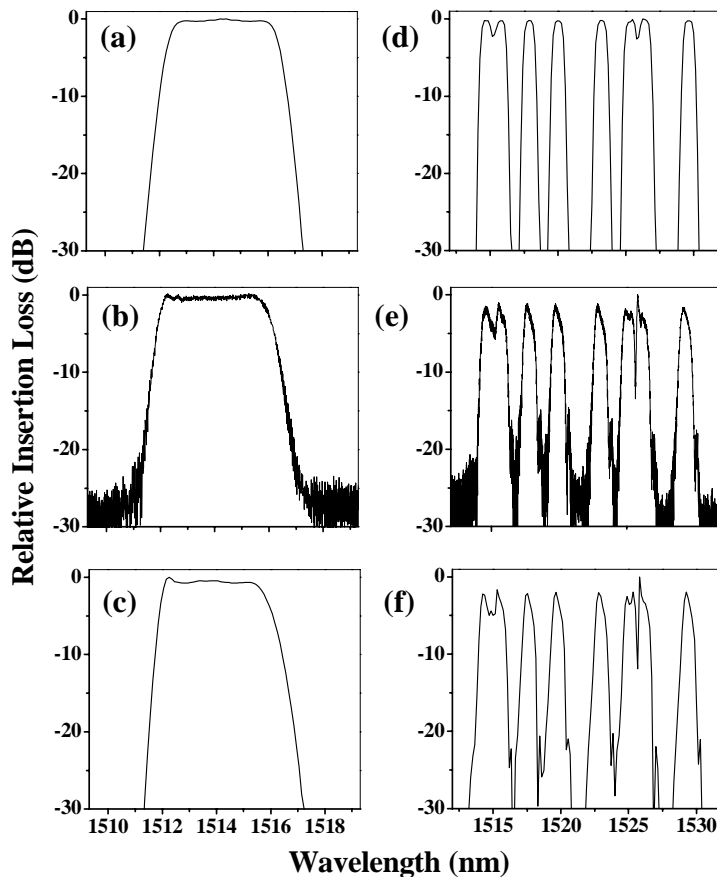


Figure 3. (a), Simulated flat-top filter with constant waveguide effective refractive index, (b), measured channel-waveguide reflection spectrum, (c), simulated flat-top filter with apodization-dependent effective refractive index; (d), simulated multi-color filter with constant refractive index, (e), measured channel-waveguide reflection spectrum, (f), simulated multi-color filter with apodization-dependent effective refractive index.

induced effective refractive index variations. In Fig. 3e, a measurement of the coder's relative reflection spectrum for TE input polarization as measured by a scanning laser source is shown. The absolute insertion loss observed including fiber coupling was about -8.5 dB implying an intrinsic device IL of about -7.5 dB. While the measured spectral bandpass of Fig 3e is in general agreement with the constant-index calculation of Fig. 2d, some distortions are evident. In Fig. 3f, a bandpass simulation based on the design set of grating lines and incorporating the small variation in effective refractive index with amplitude apodization is given. The agreement between the simulation of Fig. 3f and the measured bandpass spectrum of Fig. 3e is remarkable. It is apparent from this agreement that the photolithographic fabrication method employed reproduced the design set of grating elements with great precision. The channel-waveguide gratings studied here were designed without consideration of an effective refractive index variation with amplitude apodization. Designs can be simply corrected for the effect of apodization-induced effective refractive index changes by scaling the separation between grating lines to keep optical path distances to desired values.

Note that the insertion losses in the results reported here arise primarily from low overall reflectivity rather than true loss from scattering or other means. In reflective devices, achievable reflectivity, device length, and desired overall reflective bandwidth are strongly coupled. For fixed device length and net reflectivity, the achievable reflective bandwidth scales as the square of the intrinsic diffractive element scattering strength. Increases in index contrast and diffractive element aspect ratio are projected to expand the reflective bandwidth to values in excess of 100 nm with insertion loss of 1-2 dB.

The measurements shown in this work employ TE-polarized input signals. For TM-input polarization, the grating bandpass functions of Figure 3 were observed to shift by approximately +0.15 nm and to exhibit an additional insertion loss of ~1 dB (1.6 dB) for Figure 3b (3e). About 0.5 dB of this additional loss is attributed to a polarization dependence in the fiber-to-waveguide coupling. Measurements of 1st and 4th order unapodized reference gratings co-located in a single channel waveguide reveal polarization-mediated wavelength shifts of 0.18 and 0.15 nm, respectively. As grating-mediated wavelength shifts should be roughly four times smaller in the higher order grating, we conclude that the polarization-mediated wavelength shift stems primarily from stress and form birefringence of the waveguide. It should be noted that the presently observed sub-nm wavelength shifts do not interfere with proper operation of wide passband devices such as that demonstrated in Figure 3a-c.

III. CONCLUSIONS

In summary, we have proposed and demonstrated a novel apodization concept for lithographically-scribed channel-waveguide Bragg gratings that provides complete control over amplitude and phase of individual grating-constituent diffractive elements (lines). We have demonstrated its application to several devices with tailored spectral transfer function including a flat-top filter with steep roll-off and a multi-passband spectral decoder for optical spectral code-division multiplexing or spectral signature recognition. An amplitude-apodization-dependent variation in effective waveguide refractive index has been identified whose inclusion in design algorithms promises to provide highly accurate spectral profile realization. Overall, the precise apodization of channel waveguide Bragg reflectors via photolithographic means has been demonstrated.

REFERENCES

1. T. Erdogan, "Fiber Grating Spectra," *J. Lightwave Tech.*, vol. 15, pp. 1277-1294, 1997.
2. J. L. Rebola and A. V. T. Cartaxo, "Performance Optimization of Gaussian Apodized Fiber Bragg Grating Filters in WDM Systems," *J. Lightwave Tech.*, vol. 8, pp. 1537-1544, 2002.
3. A. Carballar, M. A. Muriel, and J. Azana, "Fiber Grating Filter for WDM Systems: An Improved Design," *IEEE Photon. Tech. Lett.*, vol. 11, pp. 694-696, 1999.
4. T. Komukai, K. Tamura, and M. Nakazawa, "An Efficient 0.04-nm Apodized Fiber Bragg Grating and Its Application to Narrow-Band Spectral Filtering," *IEEE Photon. Tech. Lett.*, vol. 9, pp. 934-936, 1997.
5. C. Marra, A. Nirmalathas, D. Novak, C. Lim, L. Reekie, J. A. Besley, C. Weeks, and N. Baker, "Wavelength-Interleaved OADMs Incorporating Optimized Multiple Phase-Shifted FBGs for Fiber-Radio Systems," *J. Lightwave Tech.*, vol. 21, pp. 32-39, 2003.
6. K. O. Hill, B. Malo, F. Bilodeau, S. Theriault, D. C. Johnson, and J. Albert, "Variable-spectral-response optical waveguide Bragg grating filters for optical signal processing," *Opt. Lett.*, vol. 20, pp. 1438-1440, 1995.
7. A. Grunnet-Jepsen, A. E. Johnson, E. S. Maniloff, T. W. Mossberg, M. J. Munroe, and J. N. Sweetser, "Fibre Bragg grating based spectral encoder/decoder for lightwave CDMA," *Electron. Lett.*, vol. 35, pp. 1096-1097, 1999.
8. D. Wiesmann, C. David, R. Germann, D. Erni, and G. L. Bona, "Apodized Surface-Corrugated Gratings With Varying Duty Cycles," *IEEE Photon. Tech. Lett.*, vol. 12, pp. 639-641, 2000.
9. D. Wiesmann, R. Germann, G. L. Bona, C. David, D. Erni, and H. Jackel, "Add-drop filter based on apodized surface-corrugated gratings," *J. Opt. Soc. Am. B*, vol. 20, pp. 417-423, 2003.
10. Y. Shibata, T. Tamamura, S. Oku, and Y. Kondo, "Coupling Coefficient Modulation of Waveguide Grating Using Sampled Grating," *IEEE Photon. Tech. Lett.*, vol. 6, pp. 1222-1224, 1994.
11. T. W. Mossberg, "Lithographic Holography in Planar Waveguides", *SPIE Holography Newsletter*, vol. 12, pp. 1 and 8, 2001.
12. C. Greiner, D. Iazikov, and T. W. Mossberg, *J. Lightwave Technol.*, accepted for publication.